Biosorption of heavy metal ions from the aqueous solutions using groundnut shell activated carbon: batch adsorption, kinetic and thermodynamic studies

Sathees Kumar V.[1], Gokulan R.[2], Geetha M. B.[3], and Zunaithur Rahman D.[4]*

[1]Department of Civil Engineering, Government College of Technology, Coimbatore 641013, Tamil Nadu, India

[2]Department of Civil Engineering, GMR Institute of Technology, Srikakulam 532127, Andhra Pradesh, India

[3]Department of Chemistry, St. Michael College of Engineering and Technology, Kalayarkoil 630551, Tamil Nadu, India
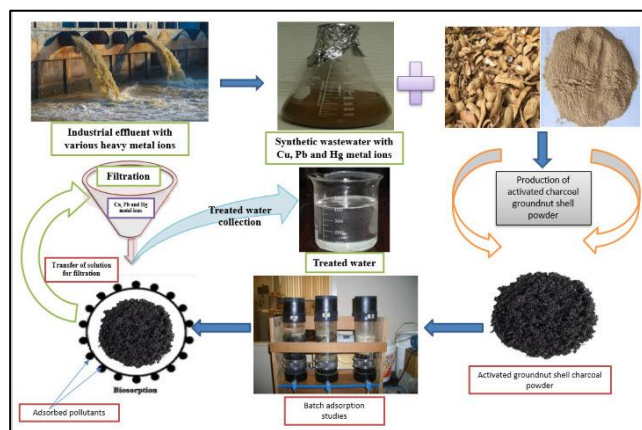
[4]Department of Civil Engineering, Aalim Muhammed Salegh College of Engineering, Avadi, Chennai 600055, India

Graphical abstract

1. Introduction

Many pollutants are released into the environment because of various industrial activities and rapid urbanization, creating many problems in the contemporary world. Apart from the organic contaminants, most are non-degradable and harmful to living beings. Heavy metals play an essential role in aqueous toxicity due to their non-degradable and poisonous nature. Usually, the pollutants of metal ions exist in the aqueous solutions because of the discharge of effluent from various industries, such as electro-plating, tanneries, smelting and alloy industries, etc., into the surface water bodies without any prior treatment. Treatment of aqueous solutions from heavy metal pollution was a difficult task in the past, and several ways have been devised to eliminate hazardous heavy metal pollution. Adsorption, Membrane filtration, Ion-exchange, Chemical precipitation, etc., are widely used to control the number of toxic metal ions from the aqueous solutions (Abdulaziz *et al.,* 2019). Excess amounts of secondary sludge generation, highly skilled workers and their needs & huge investments are needed for the above techniques. For this reason, no other process or development was seen in earlier days (Sruthi *et al.,* 2018). There is a need to develop innovative technologies to treat heavy metal pollution with meagre capital and investment costs.

To focus on the new technologies, biosorption was the best treatment technology to remove the pollutants with very low capital and investment costs. It is the process of binding contaminants (Organic/Inorganic) on the surface of the adsorbent by wan der wall's force in between the pollutants and adsorbent materials (Rice husk, Coconut Shells, Date Pits, etc.). The biosorption process has many

Abstract

Batch adsorption studies of heavy metals were carried out using activated charcoal groundnut shell powder as an adsorbent material. The groundnut shell was collected and synthesized by chemical synthesis to convert it into charcoal form. The prepared adsorbent's pore size & surface area was analyzed by BET surface analysis using N_2 – adsorption & desorption process. XRD techniques analyzed the crystalline structure of charcoal adsorbent, and the functional groups & behaviour of the surface were analyzed through FTIR, SEM, and EDX analysis. The optimum adsorption parameters of pH, temperature, time of contact between adsorbent and adsorbate, groundnut shell dose, and metal ion concentrations were obtained from the batch studies with an optimum concentration of 20 mg/L, and the mass transfer mechanism and rate-controlling step was identified by isotherm and kinetic studies. The adsorbent with the dose of 2.5 g L^{-1} removed 87.12% of Cu ions, 92.28% of Pb ions and 95.62% of Hg ions at the pH of 2.0 with 25 mg L^{-1} concentrated metal ions in the synthetic solution.

advantages no sludge production, selective pollutant removal, rapid adsorption, and desorption rate, which shows the feasibility of pollutants uptake from the aqueous solution (Idris *et al.,* 2012). One of the essential procedures in the adsorption process is selecting the adsorbent material. Many natural and inorganic adsorbents were used, showing their best ability to remove the pollutants from the water/wastewater. This study utilised ground nut husk powder as an adsorbent

material to remove hazardous metal ion concentrations from synthetic water. Groundnut hulls, also called peanut hulls, are bulky wastes during the production of peanuts, and it has lots of oil contents, minerals, and amino acids. Around 63.5% of peanuts are grown in Asia, and India produces 9 million tons of peanuts per year (An *et al.,* 2011). These peanut hulls reduce about 20% of greenhouse gas efficiency and are used for energy production.

Table 1. Various research works for the adsorption of metal ions using groundnut shells

S. No.	Metal ion	Metal ion uptake (%)	Ion concentration	Ideal pH	Groundnut shell dose	Time of contact	Reference
1.	Cu, Zn & Hg	87.12, 92.28 & 95.62	25 mg/L	6.0	2.5 g L^{-1}	60 min	In this study
2.	Cu & Pb	68.2 & 77.8	10 mg/L	5.0	50 gm & 30 gm	12 hrs.	Kalavathy *et al.,* 2014
3.	Cd, Hg & Pb	99.60, 100 & 100	0.50 mg/L	4.63	0.56 mg g^{-1}	72 min	Mehdi *et al.,* 2021
4.	Cu & Cr	25.39 & 27.86	19 mg/L	5.0	1 gm	20 min	Ashraf *et al.,* 2016
5.	Pb	71.1	5 mg/L	4.0	5 g L^{-1}	100 min	Kibami *et al.,* 2018
6.	Pb, Cu, Cd, Ni & Zn	46.7, 28.3, 18.75, 35.05, 12.65	50 mg/L	6.0	20 mg	80 min	Cobbina *et al.,* 2019
7.	Cr & Ni	76.6 & 71.2	20 mg/L	4.0	15 g L^{-1}	30 & 150 min	Bich *et al.,* 2021

Furthermore, these hulls were employed in manufacturing cosmetics, plastics, soaps, and so forth; based on their uses and production rate, they play an important part in the country's economic growth. In this study, peanut hulls were transformed into activated carbon and employed as an adsorbent material to remove the heavy metal ions Copper (II), Lead (II), and Mercury (II) from synthetic solutions. All the experiments were performed in batch mode under various operating conditions, and multiple kinetic and thermodynamic approaches evaluated the adsorption process. Table 1 represents the different heavy metal ions removed using groundnut shell powder as adsorbent material.

2.   Materials and methods

2.1. Preparation of groundnut shell adsorbent

The ground nut hulls are collected from various sources and dried at constant temperature (60°C) for up to 24 hours to remove the water contents and other pollutants. The samples were collected and washed repeatedly with distilled water before being dried in an oven at 80°C. The powder sample was crushed, taken, and kept in a beaker to make the activated carbon from the groundnut shells. 0.1 N of HCl acid was added to the beaker sample for up to 3 hours to remove the organic and other pollutants in the groundnut shell powder. The solution was filtered out with filter paper, and the sample was dried for 10 hours at 80°C. Finally, the range's dry powder was removed and used in additional studies.

2.2. Stock solution preparation

The stock solution for the entire experimental analysis has been prepared by adding 100 mg of CuSO$_4$, PbSO$_4$ & HgSO$_4$ powder with 1 litre of distilled water to obtain the adsorption efficiency of groundnut hulls. Double distilled water was used to get multiple design concentrations, and the pH adjustments were made by using 0.1 M of HCl in the entire batch mode studies.

2.3. Surface area and pore distribution

Table 2. Pore characteristics of groundnut shell charcoal adsorbent

S.No.	Parameter	Units	Groundnut shell Charcoal Adsorbent
1.	BET surface area	m^2 g^{-1}	63.442
2.	Volume of the pores	cm^3 g^{-1}	0.0978
3.	Microvolume of pores	cm^3 g^{-1}	0.201
4.	Meso volume of pores	cm^3 g^{-1}	0.095
5.	Micro area of pores	m^2 g^{-1}	316
6.	Pore radius - average	Å	16.731

The diameter of the adsorbent's pore & size, meso pore & micropore of ground nut shell ash, and its Brunauer-Emmett-Teller (BET) surface area were analyzed using the nitrogen adsorption and desorption studies under the temperature of -196°C. Referring the Figure 1, the features of groundnut shell adsorbents were obtained, and their rate of adsorption & desorption follows type – II isotherm nature. Due to multilayer adsorption, the meso pores are exhibited in the second portion of the figure at very high relative pressure. At the same time, the first part of the curve reflects the produced adsorbent's micropores (Rai *et al.,* 2016). The experimental analysis shows the results of pore volume for groundnut shell

adsorbent is around 0.0978 cm^3 g^{-1}, and the BET surface area of the adsorbent is 63.442 m^2 g^{-1}. The results confirm that the prepared adsorbent's pore size and BET area are smaller than usually activated carbons (Saeed *et al.,* 2021). The values of pore characteristics of groundnut shell adsorbent are represented in Table 2.
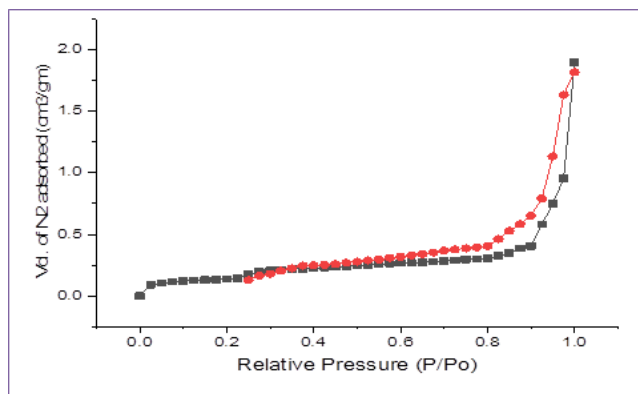

Figure 1. BET isotherm study of groundnut shell adsorbent by Nitrogen adsorption-desorption.

2.4. Batch adsorption process

Metal ions and their adsorption process using groundnut shell powder have been evaluated by the batch mode of the adsorption process under various operating conditions. The experimental analysis was performed by varying the pH, time of contact, groundnut shell powder dose, temperature & metal ion concentrations. The effect of harmful pollutant adsorption by groundnut shell powder activated carbon was tested by setting the metal ion concentration to 50 mg L^{-1} in 100 mL of synthetic solution. Using the buffer solutions, the pH level of the artificial water was adjusted from 2 – 7 at 30°C with 60 minutes of equilibrium time. Furthermore, the dose level of groundnut shell powder was raised from 0.5 g L^{-1} to 2.5 g L^{-1} for the duration of the experiment. The prepared adsorbent was poured into the prepared synthetic solutions with known concentrations. The conical flask was kept in the rotary shaker for continuous shaking to get the equilibrium for up to 60 minutes. The impact of contact time between adsorbent and metal ions varies from 10 to 120 minutes. The amount of metal ions adsorbed by groundnut shell powder activated carbon was calculated using Equation 1.

$$q_t = \frac{(C_o - C_t)\,V}{m}\ mg/g \qquad (1)$$

The metal ion and its quantity uptake by the adsorbent are represented in qt, and the concentration of the batch adsorption study is denoted in Ct. After 5 minutes of centrifugal, the final suspension was taken from the shaker and allowed into the metal ion concentration determination. The AAS (Atomic Adsorption Spectroscopy) AA6300 was used to determine the concentration of heavy metal ions in the aqueous solution before and after equilibrium. Each analysis was performed up to 2 times, and the concurrent values were considered. The mass balance system for this adsorption process can be expressed in equation 2.

$$\%\ Removal = \left[\frac{C_o - C_e}{C_o}\right] X100 \qquad (2)$$

The initial metal ion concentrations in the aqueous solutions are represented by C$_o$ & final concentrations are represented by C$_e$ at the time of equilibrium level of metal ion solution in mg L^{-1}. The solution's volume is represented by V & mass of the adsorbent used in the solution is represented by m.

2.5. FTIR studies

Fourier Transform Infrared Spectroscopy (FTIR) analysis was used to evaluate the functional group characterization and its presence in the groundnut shell adsorbent. The chemical characteristics of the prepared adsorbent were also identified by this method (Chen *et al.,* 2017). The synthetic solution with a concentration of metal ions of 25 mg L^{-1} was combined with 1 gm of produced groundnut powder adsorbent, and the pH of the solution was 6.0. The rotary shaker was set to a continuous agitation speed of 200 rpm, and the suspension was left on the conical flask for up to 4 hours. The final suspension was taken after 4 hours and used for further experimental works. The FTIR scanning range was adjusted from 400 to 4000 cm^{-1} with a resolution of 4 cm^{-1}, and the spectra were produced by scanning up to 20 times. The functional groups and their characterization were used to check the ability of binding nature of the adsorbent.

2.6. SEM/EDX analysis

Using JSM – 6940V, Scanning Electron Microscope (SEM) & Energy Dispersive X-ray (EDX) spectroscopy, activated groundnut shells' elemental and physical nature were examined under various operating conditions. Defects and fractions on the adsorbent's surface were found at a working distance of 20 μm with a voltage level of 15 kV. The EDX analysis was performed to confirm the adsorption of the appropriate metal ions.

2.7. XRD analysis

Under different peak levels, the crystalline structure and intensity of groundnut shell adsorbent were evaluated by X-ray Diffraction Analysis (XRD). The XRD instrument was operated with the CuK-α radiation and 40 kV power at a 250-mA working level. The phases and structure of the groundnut shell adsorbent were observed. Referring to the JCPDS standards, the peaks obtained from the XRD were in good agreement with the reference code -00-002-1035 (Manjuladevi *et al.,* 2018).

2.8. Isotherm studies

The adsorption isotherm studies have investigated the transmission of targeted metal ions from the solution phase to the adsorbent during the equilibrium state. This may help to identify the interaction between adsorbents and their optimization during adsorption. The following are the types of isotherm studies used widely to evaluate the performance of the adsorption process in batch mode.

2.8.1. Langmuir isotherm

Langmuir isotherm analysis was used to characterize the equilibrium between the adsorbate and adsorbent systems. Two assumptions underpin the isotherm study. The whole adsorption process, in other words, comprises a monolayer on the adsorbent surface, making molecular interaction at multiple places impossible (Sapna *et al.,* 2018). Equation 3 expresses the Langmuir isotherm model.

$$\frac{C_e}{q_e} = \frac{1}{K.q_{max}} + \frac{C_e}{q_{max}} \tag{3}$$

C_e – Concentration of equilibrium of the adsorbate solution

q_e – Amount of groundnut shell powder adsorbed per gm.

K & q_{max} – Constants of Langmuir isotherm equation related to capacity and intensity of adsorption

2.8.2. Freundlich isotherm

The Freundlich isotherm analysis can clearly describe the adsorption behaviour of the process. Freundlich isotherm follows the multilayer adsorption system on the adsorbent surface and mainly occurs on heterogeneous surfaces (Sivakumar *et al.,* 2015). Equation 4 expresses the Freundlich isotherm model.

$$\ln q_e = \ln k_f + \frac{1}{n}\ln C_e \tag{4}$$

q_e – Adsorbed quantity of adsorbate per gm; n – Adsorption Energy; K_f – Capacity of adsorption related to Freundlich constant; C_e – Adsorbate solution's equilibrium concentration.

2.8.3. Sips isotherm

The Langmuir and Freundlich isotherm models were integrated to forecast the adsorption process in the heterogeneous mixed isotherm system. The sips model forecasts monolayer adsorption when the concentration of the solution is very high (Melánia *et al.,* 2021). Also, the solution's attention is completely avoided and follows the Langmuir model. The expression for the sips isotherm model can be expressed in equation 5.

$$\frac{1}{q_e} = \frac{1}{Q_{max}K_s}\left(\frac{1}{C_e}\right)^{\frac{1}{n}} + \frac{1}{Q_{max}} \tag{5}$$

Q_{max} & K_s – The slope and intercept of linear plots are used to calculate the adsorption capacity, and the equilibrium constant & n - factor of heterogeneity lie between 0 to 1.

2.8.4. Toth isotherm

This type of isotherm model has been used widely for solid surfaces of homogeneous nature. Toth isotherm is usually called a three-parameter isotherm model, which is used to integrate the collaboration between the adsorbed pollutants. The Toth model provides high accuracy even in low concentrations (Senthil *et al.,* 2017). Equation 6 expresses the expression for the Toth isotherm model.

$$\ln\frac{q_e}{q_m - q_e} = n\ln K_L + n\ln C_e \tag{6}$$

K_L & n is called Toth isotherm constant in mg g^{-1} and q_e – quantity of materials adsorbed in equilibrium mg L^{-1}.

2.8.5. Redlich-Peterson (R-P) isotherm

This is commonly referred to as a three-parameter isotherm model, and the parts of this study were drawn from the Langmuir and Freundlich isotherms. The usual assumptions of the R-P isotherm model (Dalia *et al.,* 2016) are that the adsorption mechanism is unique and there is no monolayer development on the adsorbent surface. Equation 7 expresses the expression for the R-P isotherm model.

$$\ln(K_R\frac{C_e}{q_e} - 1) = b_R\ln C_e + \ln a_R \tag{7}$$

K_R – adsorption capacity constant of R-P isotherm obtained from the linear plots; a_R – R-P isotherm constant; b_R – Exponent value (0 to 1).

2.9. Kinetic studies

A line or curve indicates the aqueous medium's retention rate or solute release to the solid-phase boundary at a given pH, temperature, dosage, and flow rate. Kinetic studies identify the pollutant's uptake concerning time with fixed concentration or pressure (Nouf *et al.,* 2021). Also, kinetics is employed to analyze the adsorbate diffusion in the adsorbent pores. The following are the common types of kinetic studies that were used in the batch adsorption process.

2.9.1. Pseudo-first-order studies

The Lagergren model, also known as first-order pseudo kinetics, is based on the basic assumptions that the difference in saturation concentration is directly proportional to the rate of change in solute and solid absorption with time applicable to the early stage of the adsorption process (Shahriar *et al.,* 2020). The initial and equilibrium concentrations and their differences (q_e - q) shall be used to identify the function of adsorption. The Lagergren model linear study can be expressed in equation (8).

$$\log(q_e - q) = \log q_e - \frac{k}{2.303}t \tag{8}$$

2.9.2. Pseudo-second-order studies

By assuming that the rate of adsorption and its modulation are chemical processes, the second-order pseudo-kinetic model predicts the nature of the entire adsorption process. The adsorption capacity determines the adsorption rate, and the adsorbate concentration is unimportant (Davut *et al.,* 2020). The adsorption rate determines the number of squares in occupied sites. Equation 9 expresses the pseudo-second-order linear research.

$$\frac{t}{q}=\frac{1}{h}+\frac{1}{q_e}t \qquad (9)$$

h = kq$_e$^{2} – Initial adsorption rate and k – rate constant.

2.9.3. Boyd kinetic studies

The slowest step of metal ions on the adsorbent's surface was studied using Boyd's kinetic model. The linear graphs of this kinetic model pass through the origin, suggesting that the mass transfer rate governs the adsorption process. If the plots are linear and do not pass through the origin, the adsorption process is handled by film diffusion (Nurul *et al.*, 2020). This model was used to find an adsorbent's rate-controlling step, and the linear equation of the Boyd kinetic model may be found in equation 10.

$$Bt =-0.4977-\ln(1-F) \qquad (10)$$

B$_t$ is the function of boyd kinetic model, and F is the solute's fraction adsorbed at various times t.

2.9.4. Elovich studies

Based on specific assumptions, the Elovich kinetic model was utilized to analyze the adsorption process's performance. The main concept of this model is that as the amount of adsorbed solute increases, so does the adsorption rate (Thi *et al.*, 2015). Equation 11 expresses the Elovich kinetic research linear model.

$$q_t =\frac{1}{b}\ln(1+abt) \qquad (11)$$

a and b are the parameters obtained from the model in mg g^{-1} min^{-1} and g mg^{-1}, respectively.

2.9.5. Intra Particle Diffusion (IPD) studies

The IPD should apply only when the solute concentration in the batch adsorber is sufficiently large (Dongxiao *et al.*, 2019). The IPD model can be expressed in equation 12:

$$q_t =k_p t^{\frac{1}{2}}+C \qquad (12)$$

q$_t$ – Amount of metal ions adsorbed at time 't' in mg g^{-1}

k$_p$ – IPD rate constant

C - Intercept

2.10. Thermodynamic studies

The Gibbs energy (ΔG°), changes in enthalpy (ΔH°), and changes in entropy (ΔS°) are the three critical parameters were used to find out the exothermic or endothermic nature of the adsorption process. The parameters above were calculated using equations 13, 14 & 15.

$$K_c =\frac{C_{Ae}}{C_e} \qquad (13)$$

$$\Delta G_0 =-RT\ln K_C \qquad (14)$$

$$\log K_c =\frac{\Delta S^0}{2.303R}-\frac{\Delta H^0}{2.303RT} \qquad (15)$$

The constant of equilibrium is denoted as Kc, metal ion concentration & its equilibrium is represented as C$_e$, the quantity of metal ions uptake by the adsorbent in one litre of solution at the equilibrium is denoted as C$_{Ae}$ (mg L^{-1}), constant for the gas is taken as R = 8.314 J mol^{-1} K-1 and temperature for this process is represented as t.

2.11. Desorption process

To make the process of metal ion uptake cost-effective, we need to renew the spent adsorbent using the desorption process. Also, the disposal of adsorbed metal ions is essential. The desorption studies were carried out using 0.1 – 0.4 N of HCl, and the spent groundnut shell adsorbent was dumped in a remote location to avoid creating toxic effects. The desorption of metal ions using the groundnut shell powder adsorbent and its behaviour is directly proportional to the adsorption process.

3. Results and discussion

3.1. Characterization studies

The properties of sugarcane bagasse charcoal adsorbent material are important in batch adsorption investigations. A characterization study was typically used to confirm the ability of a material to remove targeted pollutants. In this process, the following analysis has tested the property and functional groups of the material using the subsequent investigation.
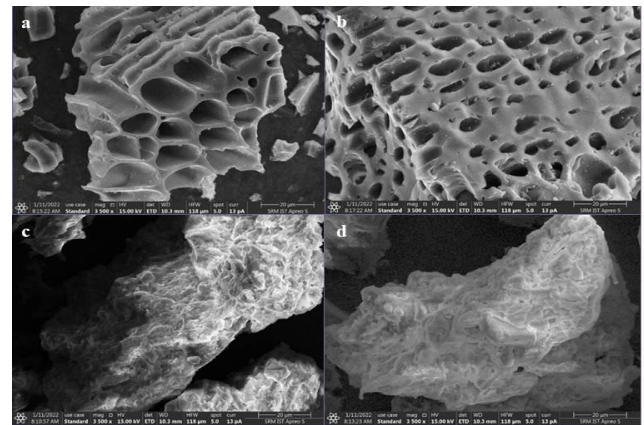
3.2. SEM analysis

Figure 2. SEM images of Groundnut shell charcoal (a) before pollutants uptake & (b) after pollutants uptake

Figures 2(a) and (b) show a scanning electron microscopic picture of groundnut shell powder adsorbent before and after metal ion adsorption from an aqueous medium. In Figure 2(a), the presence of pores and other particles is seen in the picture, and the acid activation process generates these pores through concentrated HCl. The SEM picture of the activated carbon adsorbent revealed the existence of a large surface area and active sites for the adsorption of contaminants from the aqueous medium. Also, the BET surface area analysis confirms that the activated groundnut shell adsorbent has a very high

surface area compared to other commercial activated carbons. Figure 2(b) shows the SEM image of ground nut shell charcoal adsorbent after receiving the pollutants from the synthetic solution. The presence of uneven pores on the surface of groundnut shell charcoal powder receives the contaminants at the inner walls, and all the pores are filled by the pollutants, which forms a cloud nature on the top surface of the adsorbent (Indhumathi *et al.,* 2014). Figure 2 (a) demonstrates that the adsorption process was finished since there are no unoccupied spots on the top of the adsorbent surface. These experiments indicated that contaminant adsorption occurs on the adsorbent surface due to high attraction forces (Ting *et al.,* 2018). To ensure the targeted metal ions (Cu, Pb, and Hg) and the EDX analysis may identify their adsorption on the surface of the adsorbent.
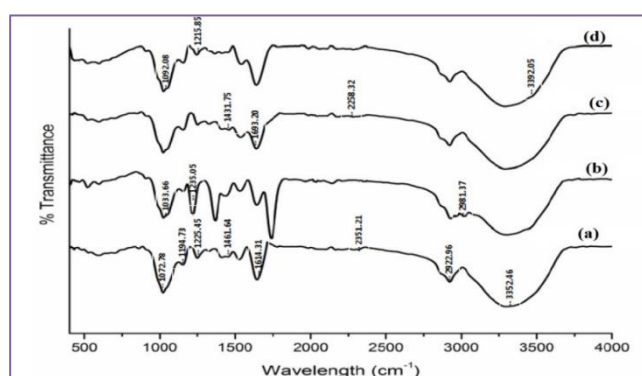
3.3. FTIR studies

Figure 3. FTIR analysis of groundnut shell powder (a) before adsorption, (b) adsorption

Figure 3 depicts the FTIR spectra of groundnut shell charcoal activated carbon and metal ions (Cu, Pb, and Hg) adsorbed groundnut charcoal carbon. The band at 3392 cm^{-1} in the figure depicts the alcohol and water stretching functional groups. The existence of an aromatic ring may confirm the occurrence of a second peak at 3352 cm^{-1} due to the -CH stretch. The peaks at 2922 cm^{-1}, 2981 cm^{-1}, 2351 cm^{-1}, and 2252 cm^{-1} were detected in the figure, demonstrating the occurrence of symmetrical bending owing to O-H stretching (Frutos *et al.,* 2016). Because of the carbonyl group, the ring vibration was seen at the peaks of 1693 cm^{-1} and 1614 cm^{-1}. Furthermore, the -CH$_2$ bending vibrations are visible in the peaks obtained at 1461 cm^{-1} and 1431 cm^{-1}. Other peaks at 1225, 1235, and 1215 cm^{-1} imply C-N stretching, whereas the peak below 1092 cm^{-1} shows functional group -COO stretching. According to the experiment's results, functional groups in activated groundnut shell powder proved their potential to adsorb contaminants.

3.4. EDX analysis

The various components existing in the synthetic solution, along with the targeted metal ions (Cu, Pb, and Hg) and their amount of adsorption, have been investigated by EDX analysis. Figure 4(a) shows the EDX image of activated groundnut shell adsorption before removing pollutants and metal ions. This picture observed the presence of

various organic and inorganic compounds such as carbon, oxygen, calcium, etc. The prepared synthetic solution was allowed into the adsorbent bed its EDX image was analyzed. Figure 4(b) shows the EDX image of the groundnut shell adsorbent after receiving the pollutants and chemical contaminants from the aqueous solutions. Referring to Figure 4(b), targeted metal ions (Cu, Pb, and Hg) were identified along with other organic and inorganic pollutants. The above experimental study confirms the adsorption nature of prepared groundnut shell adsorbent and its ability to receive the organic contaminants from the aqueous solutions (Pezhman *et al.,* 2019).
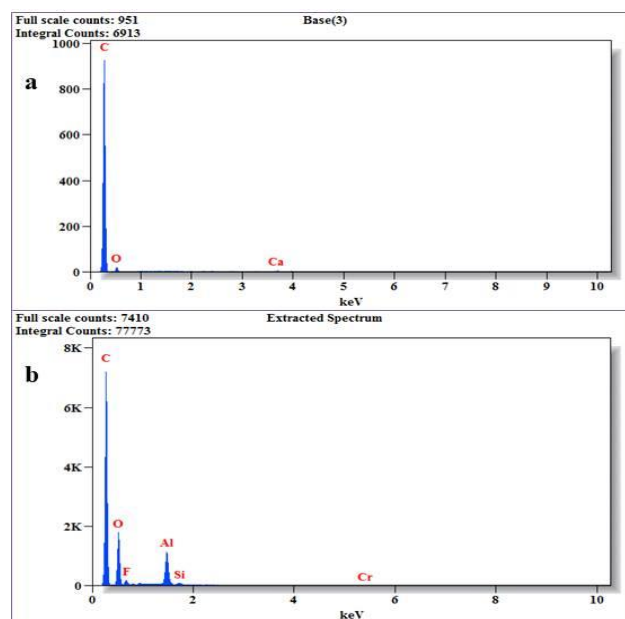

Figure 4. EDX analysis of groundnut shell powder (a) before adsorption, (b) adsorption.
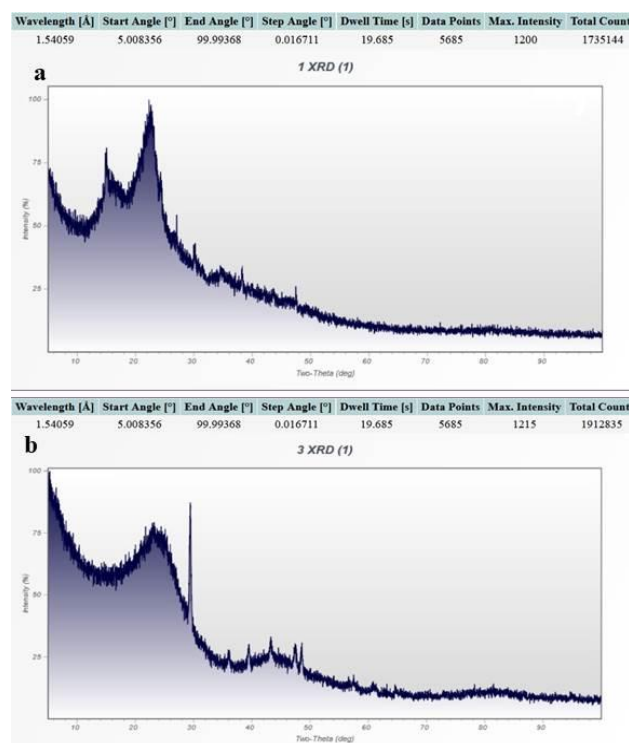
3.5. XRD analysis

Figure 5(a) & (b) represents the XRD spectra of raw groundnut shell charcoal and metal ions loaded groundnut shell charcoal, respectively. Referring to Figure 5(a), a high number of peaks was observed, and the intensity was also very high. But, referring to Figure 5(b), the peaks were shifted, and the intensity was reduced. Furthermore, peaks disappeared due to metal ion uptake on the adsorbent surface. The difference between peaks and intensity confirms the targeted metal ions (Cu, Ph, and Hg) adsorption from the aqueous solution. In XRD analysis, shifting the peaks from one position to another indicates the unit cell contraction, and a decrease in intensity and disappearance of the peak confirms the crystallinity losses of the adsorbent material (Uduakobong *et al.,* 200). The existence of micro and meso pores on the adsorbent surface diffuses and adsorbs the targeted metal ions by physical or chemical adsorption. The peaks at $2\theta = 18°, 24°, 28°, 32°, 40°,$ and $48°$ show the crystalline structure of activated groundnut shell charcoal adsorbent before taking up pollutants from the aqueous solutions.
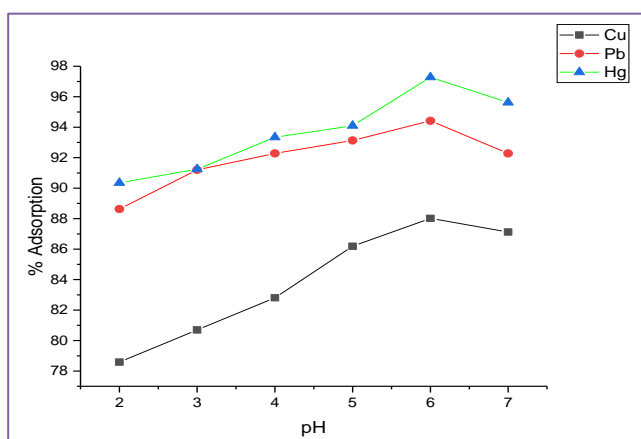
3.6. Effect of pH

Figure 6. Influence of pH in metal ion adsorption.

The pH of the synthetic solution was changed from 2.0 to 7.0. The quantity of metal ion absorption due to pH fluctuations in the solution has been studied under various operating circumstances. The concentration of each metal ion in the solution was held constant at 25 mg L^{-1}, and the dose of groundnut shell charcoal was fixed at 2 g L^{-1} throughout a 60-minute contact period. The variations in adsorption due to a rise in pH were investigated. Figure 6 shows the amount of metal ions uptake by the adsorbent with an increase in the solution's pH. When the pH of the solution was increased, the amount of adsorption also increased due to the presence of charged adsorbents of positive nature and their interface with groundnut shell charcoal adsorbent. When the pH of the solution is very high, the surface of the adsorbent has a strong positive charge, simulating fast

metal ion elimination (Gopal *et al.,* 2016). Referring to Figure 6, the maximum amount of metal ion uptake by the adsorbent was achieved at the pH of 6.0; beyond that, it was noticed that a gradual decrement in metal ion removal. The precipitation of hydroxides in higher pH values and its attribution and adsorption of metal ions decreased. The groundnut shell powder activated carbon adsorbs 87.12% of Cu ions, 92.28% of Pb ions, and 95.62% of Hg ions at the optimum pH of 6.0.

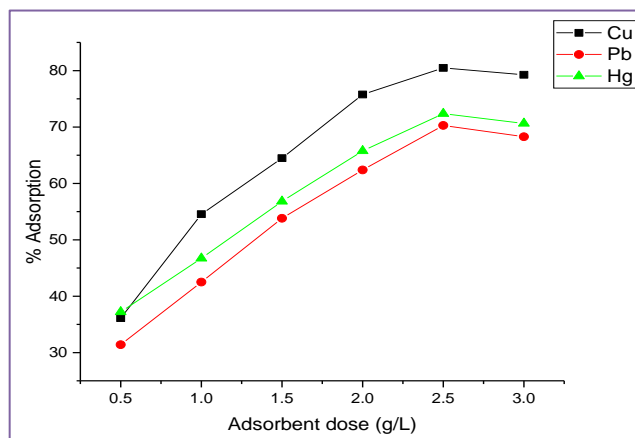### 3.7. Effect of adsorbent dose

Figure 7. Influence of adsorbent dose in metal ion adsorption.

The charcoal and concentrations of groundnut shell powder have a vital influence on the pollutant adsorption in the synthetic solution. The adsorbent dosage level was changed from 0.5 g L^{-1} to 3.0 g L^{-1} in this batch mode of investigation by keeping the solution pH at 6.0, the synthetic solution's concentration at 25 mg L^{-1}, and the contact period at 60 minutes. Referring to Figure 7, the metal ion uptake from the synthetic solution has increased with the increase in groundnut shell charcoal adsorbent. The highest adsorption efficiency was observed at a dosage level of 2.5 g L^{-1}. Beyond that, the concentration gradient and its decrease have little effect on metal ion adsorption from aqueous solutions. The increase in metal ions uptake with an increase in groundnut shell charcoal adsorbent due to the free active surface availability to adsorb the molecules (Pongthipun *et al.,* 2021). In this study, 2.5 g L^{-1} of charcoal adsorbent adsorbs 80.48% of Cu, 70.28% of Pb, and 72.37% of Hg metal ions from the aqueous solutions.

3.8. Effect of contact time

The quantity of pollutant uptake in the adsorption process is affected by the contact time between two reactions. The concentration of metal ions in the synthetic solutions was changed from 25 mg L^{-1} to 150 mg L^{-1} in this investigation by adjusting the contact period from 10 to 120 minutes with a pH of 6.0 solution and a groundnut shell charcoal dosage of 2.5 g L^{-1}. Referring to Figure 8, the amount of metal ion uptake during the initial stages was very rapid because of the availability of active/vacant sites in the adsorbent. The adsorption process reached a saturation level in the mesopores. The figure shows that

the maximum efficiency was obtained within 60 minutes. Apart from that, due to the repulsive force on the surface of adsorbent molecules, the amount of metal ion absorption by the adsorbent stays constant (Varney et al., 2021). Mass transfer between solid and liquid phases has slowed with time. Pollutants require great energy to penetrate the pores in the final stages, reducing adsorption efficiency.
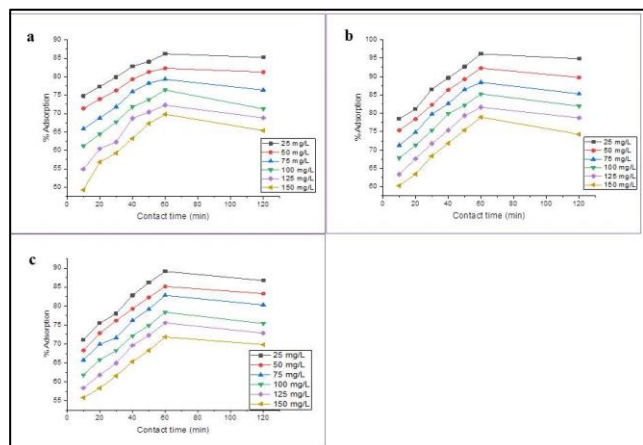

Figure 8. Influence of contact time for the adsorption of (a) Cu, (b) Pb and (c) Hg metal ions.

3.9. Effect of metal ion concentrations

The concentration of metal ions in the aqueous solution creates a vulnerable nature and toxic effects on the surroundings. It also influences metal ion absorption by the activated adsorbent material. The concentration of

each metal ion was changed from 25 to 150 mg L^{-1} in this investigation, and the behaviour of adsorption efficiency was also observed. The influence of different metal ion concentrations on adsorption performance was investigated using a pH of 6.0 solution, a groundnut shell charcoal dosage of 2.5 g L^{-1}, and a contact period of 60 minutes. Referring to Figure 9, it was seen that the metal ion uptake was rapid at low concentrations of metal ions. When the ion concentration in the solution increased gradually, the metal ion uptake was slowly reduced. Because of the abundance of large active sites at low metal ion concentrations, the adsorption process was quick. Metal ions absorbed by the adsorbent become saturated in the mesopores (Yogeshwaran *et al.,* 2021). In this batch study, 25 mg L^{-1} concentrated metal ion solution provides high adsorption efficiency using groundnut shell charcoal powder. Up to 98.63% of Cu, 87.29% of Pb, and 82.83% of Hg metal ions were adsorbed using the activated adsorbent material in low concentrations. The amount of metal ion uptake by the groundnut shell powder was rapid in lower concentrations, which indicates the adsorbent has not stretched the overload level.

3.10. Isotherm studies

The adsorption process's behaviour and features were analyzed using five distinct types of isotherms models. The temperature was kept at 30°C in this investigation, while the other parameters were selected from the optimal values from batch experiments. An isotherm suiting the adsorption type was discovered using the regression values obtained from the linear plots.

Table 3. Adsorption isotherm constants for metal ion adsorption using groundnut shell charcoal adsorbent

S. No.	Model	Parameters	Cu	Pb	Hg
1.	Langmuir	q_{max}	9.402	9.929	10.434
		K_L	0.343	0.174	0.109
		R^2	0.9721	0.9505	0.9473
2.	Freundlich	K_f	2.541	1.832	1.389
		n	2.963	2.315	2.026
		R^2	0.9546	0.9602	0.9912
3.	Redlich-Peterson (R-P)	K_{RP}	11.325	6.28557	4.5350
		α_{RP}	0.32684	0.13132	0.0744
		β_{RP}	1.05217	1.14532	1.2139
		R^2	0.9571	0.9875	0.9868
4.	Sips	K_S	12.8689	6.13959	3.7113
		β_S	1.25346	1.54742	1.6536
		a_S	0.47347	0.24345	0.1544
		R^2	0.9182	0.9599	0.9991
5.	Toth	Qmax	27.4598	25.4221	24.0547
		b_T	0.38393	0.22272	0.1699
		n_T	0.78414	0.58286	0.4973
		R^2	0.8287	0.8224	0.829

3.10.1. Langmuir isotherm

The slope and deflection data from the linear isotherm plot of C_e/q_e vs C_e were used to calculate the Langmuir isotherm constants. The linear plots of the Langmuir isotherm study are shown in Figure 10(a), and the values

of the constants (k, q_{max}) are determined and presented in Table 3. At 30°C temperature, the regression values obtained and listed in Table 3, which are higher than the average values ($R^2 > 0.95$), indicate the applicability of this isotherm model. The computed separation values for 25

mg L^{-1} metal ion concentration range from 0 to 1, validating the monolayer adsorption process in physical or chemical mode (Jabbar *et al.,* 2016).

3.10.2. Freundlich isotherm

This isotherm allows for multilayer adsorption in either physical or chemical mode. Figure 10(b) shows the linear plots ln q_e vs ln C_e at 30°C, and Table 3 shows the isotherm constants K_f and n values. The constant value n ranges from 1 to 10 and may support the physical adsorption of metal ions by groundnut shell charcoal powder. The comparable experimental data fits both the Langmuir and Freundlich isotherm models perfectly. Furthermore, the regression values (R^2) computed from the linear plots are well-matched with both isotherm models, demonstrating the usefulness of isotherm models.
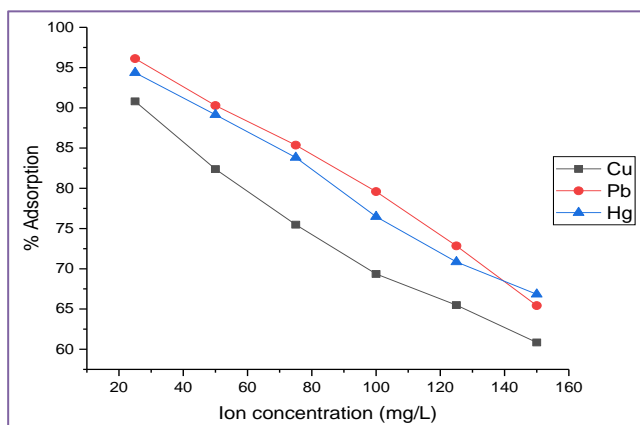

Figure 9. Influence of metal ion concentration in adsorption.

3.10.3. Sips isotherm

The Langmuir and Freundlich isotherm models were used to create this sort of isotherm. The constants of this isotherm model (Q_{max} & K_s) were determined using slope and deflection measurements from the sips model linear charts. The linear fit in Figure 10(c) supports the applicability of this isotherm model for the adsorption process. Table 3 shows the values of constants and regression coefficients. The heterogeneity factor (n) is between 0 and 1, and R^2 values greater than 0.95 suggest that this model fits (Rahim *et al.,* 2021). The sipping model equation simplifies to the Langmuir isotherm equation if n = 1 and to the Freundlich isotherm equation if n = 0.
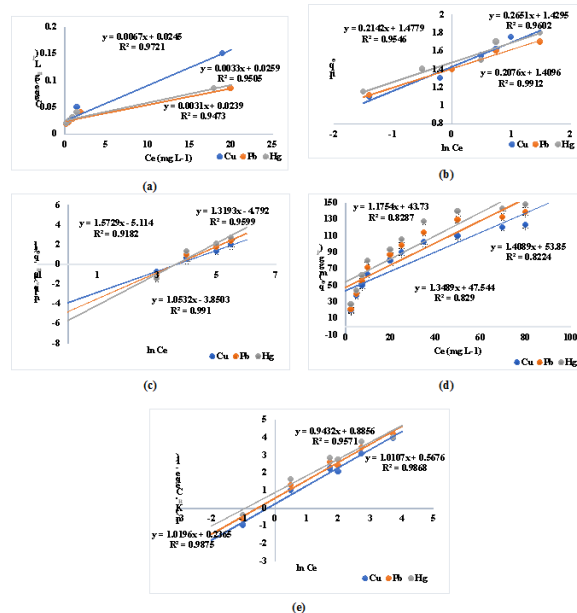

Figure 10. Adsorption isotherm plots for (a) Langmuir, (b) Freundlich, (c) Sips, (d) Toth & (e) R -P models for metal ion uptake using groundnut shell adsorbent.

3.10.4. Toth isotherm

The presence of heterogeneous solid surfaces has been identified using the Toth isotherm model. Figure 10(d) shows the linear plots for the Toth isotherm model, and its constants are listed in Table 3. Toth isotherm model is usually called a three-parameter model, used to identify the effects of the interaction between adsorbed surfaces and the metal ions (Wilson *et al.,* 2020). The regression values (R^2) obtained from the linear plots of the Toth isotherm model are very low (< 0.95), and it indicates the non-applicability of isotherm fitting. If the Langmuir or Freundlich isotherm data was not fitted with the adsorption process, the Toth isotherm might be used for connecting the equilibrium data.

3.10.5. R-P isotherm

The R-P isotherm model provides good quality results with very high accuracy compared to other isotherm studies because of the requirement of three unknown values (Jiao *et al.,* 2012). The linear plots of this isotherm model are shown in Figure 10(e), and the slope & deflection values were obtained and represented in Table 3. The b_R values from the table lying between 0 to 1 may confirm the applicability of this isotherm model. If b_R = 1, the equation becomes Langmuir fit, and b_R = 0, the equations become Freundlich fitting of the isotherm. The batch studies' experimental findings fit well with Langmuir, Freundlich, Sips, and R-P isotherm investigations. The best fit for metal ion adsorption using groundnut shell charcoal powder is determined by the R^2 values derived from the linear plots of each isotherm model; Langmuir > Freundlich > R- P > Sips. From the isotherm studies and fitting of various isotherm models, the adsorption process follows a heterogeneous and monolayer adsorption mechanism.

3.11. Kinetic studies

The kinetic studies of the batch adsorption process have been evaluated under various concentrations of metal ions in the aqueous solutions. The results obtained from the batch mode were used for five different kinetic studies to assess the process of metal ion uptake by the adsorbent material. The constants of each kinetic study have been evaluated from the slope deflection values by referring to the linear plots. The regression values were obtained from the linear plot, confirming the fitting of the best kinetic model. The following are the adsorption kinetic studies used to identify the adsorption process in this batch study.

3.11.1. Pseudo First order model

Figure 11 depicts the pseudo-first-order or Lagergren model's linear plots [(q_e - q) vs t]. The concentration of metal ions was adjusted from 25 to 150 mg L^{-1}, and the linear plots of the equation yielded the first-order rate

constant (k) and R^2 values. This model's constants were determined and displayed in Table 4, and R^2 values were found to be quite high (> 0.95). This validates the Lagergren model's applicability in the adsorption process, implying that the adsorption process has achieved saturation (Renu *et al.*, 2020).

3.11.2. Pseudo second order model

The linear plots of the pseudo-second-order equation are shown in Figure 12, and the constants of this model were determined from the slope and deflection values of the linear plots and are shown in Table 4. The experimental q_e values obtained are virtually identical to the estimated q_e values from the table, confirming the applicability of the pseudo-second-order kinetic model in batch adsorption studies. Furthermore, the regression values (R^2) were high, indicating the adsorption process had achieved equilibrium (Xiao *et al.*, 2014).

Table 4. Adsorption kinetic constants and parameters using various kinetic models

S.No.	Type of metal	Conc. (mg/L)	Pseudo 1st order			Pseudo 2nd order			Elovich			Boyd			Intra-particle diffusion		
			K (min^{-1})	q_e, cal (mg/g)	R^2	K (g/mg. min) X 10^{-3}	q_e, cal (mg/g)	h (mg/g.min)	R^2	a (mg/g. min)	b (g/mg)	R^2	B	D_i (x 10^{-3} m^2/s)	R^2	K_p (mg/g.min$^{1/2}$)	C	R^2
1.	Cu	25	0.034	2.64	0.95	16.69	2.15	0.10	0.96	0.244	1.55	0.94	0.034	5.472	0.915	0.197	0.41	0.95
2.		50	0.043	7.02	0.93	5.73	5.19	0.18	0.98	0.988	0.74	0.93	0.044	7.340	0.973	0.399	0.58	0.95
3.		75	0.041	10.00	0.93	3.34	8.30	0.22	0.98	0.978	0.55	0.92	0.043	7.621	0.963	0.517	0.60	0.98
4.		100	0.039	11.36	0.94	5.07	10.75	0.26	0.98	0.948	0.44	0.95	0.039	6.856	0.914	0.783	0.54	0.99
5.		125	0.048	17.47	0.92	2.00	12.91	0.29	0.97	0.977	0.35	0.92	0.049	8.725	0.982	0.804	0.37	0.93
6.		150	0.045	19.43	0.93	3.12	13.82	0.30	0.96	0.934	0.26	0.92	0.045	7.452	0.952	0.856	0.32	0.96
7.	Pb	25	0.046	3.68	0.91	12.62	2.70	0.10	0.97	0.263	1.16	0.91	0.046	7.678	0.943	0.190	0.38	0.98
8.		50	0.041	6.54	0.93	5.32	5.47	0.12	0.98	0.328	0.81	0.94	0.041	6.294	0.983	0.348	0.51	0.94
9.		75	0.043	9.95	0.92	3.56	8.60	0.23	0.98	0.541	0.65	0.93	0.045	7.959	0.924	0.554	0.68	0.95
10.		100	0.046	12.38	0.94	2.77	10.10	0.28	0.97	0.611	0.47	0.92	0.046	7.678	0.983	0.686	0.67	0.95
11.		125	0.052	20.55	0.92	2.30	11.56	0.31	0.98	0.618	0.31	0.90	0.053	8.590	0.941	0.772	0.51	0.97
12.		150	0.050	25.48	0.94	2.65	12.73	0.33	0.96	0.596	0.20	0.92	0.055	8.972	0.922	0.805	0.32	0.96
13.	Hg	25	0.039	2.84	0.95	15.43	2.14	0.09	0.96	0.230	1.63	0.94	0.037	6.428	0.993	0.189	0.30	0.97
14.		50	0.032	6.51	0.93	5.31	5.55	0.15	0.99	0.323	0.87	0.96	0.041	6.492	0.939	0.318	0.37	0.98
15.		75	0.041	10.40	0.91	3.64	7.74	0.21	0.97	0.484	0.65	0.94	0.046	7.687	0.920	0.514	0.42	0.94
16.		100	0.044	13.27	0.95	2.86	9.40	0.27	0.98	0.572	0.46	0.93	0.050	8.344	0.942	0.677	0.41	0.95
17.		125	0.044	18.35	0.94	1.35	12.64	0.23	0.98	0.652	0.36	0.92	0.049	8.725	0.941	0.746	0.32	0.96
18.		150	0.051	23.47	0.95	1.11	15.23	0.25	0.95	0.549	0.25	0.91	0.045	8.921	0.955	0.840	0.27	0.97

3.11.3. Boyd kinetic model

Figure 13 shows linear graphs of B_t vs t demonstrating the linearity of the Boyd kinetic model. According to the illustration, the plots are in linear shape and fail to pass through the plots' origin. The groundnut shell charcoal powder regulates the process of metal ion absorption by film or external diffusion (John *et al.*, 2020). The Boyd kinetic constants (D_i & B) were determined using the slope and intercept of linear plots and are shown in Table 4. The regression results (R^2) of this kinetic model are presented in the table, confirming the kinetic model's non-applicability in this batch research.

3.11.4. Elovich kinetic model

The kinetics of metal ion adsorption using groundnut shell charcoal powder was investigated by graphing q_t vs ln t using the Elovich model. Figure 14 depicts the linear plots of the Elovich kinetic model, and the constants (a & b) were computed using the slope and deflection values of the linear plots. This model's fundamental premise is that the chemical adsorption of gases on heterogeneous adsorbent surfaces does not allow for any process (Risha *et al.*, 2021). Table 4 shows the regression values (R^2) of

the Elovich model, which are shown to be high, confirming the applicability of this kinetic model.

3.11.5. IPD kinetic model

Figure 15 shows the IPD kinetics model's linear plots of q_t vs $t^{0.5}$, which reveals that metal ion adsorption was governed by intra-particle diffusion owing to plots passing through the origin point. The two or more phases of the adsorption cycle are represented by the multilayer structure of data curves (Venkatraman *et al.*, 2021).
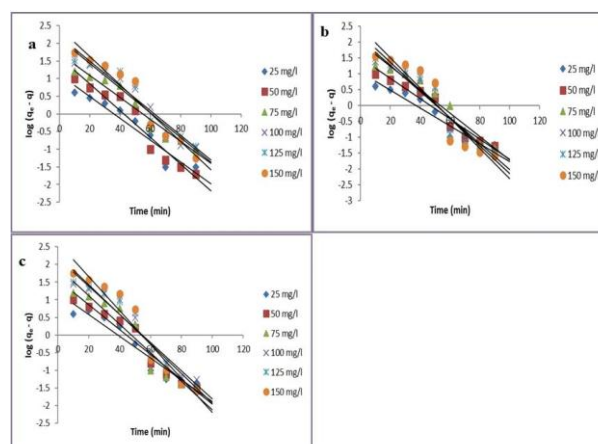
Figure 11. Pseudo 1st order plots of (a) Cu, (b) Pb and (c) Hg metal ion adsorption using groundnut shell powder.
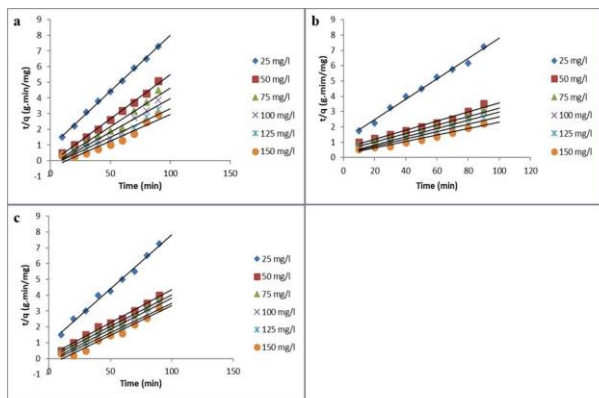

Figure 12. Pseudo 2nd order plots of (a) Cu, (b) Pb and (c) Hg metal ion adsorption using groundnut shell powder.
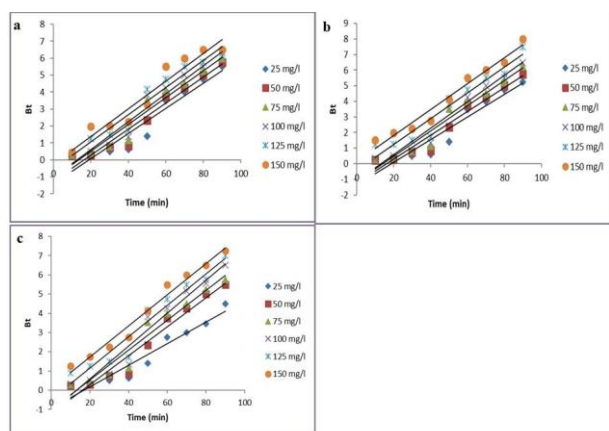

Figure 13. Boyd kinetic plots of (a) Cu, (b) Pb and (c) Hg metal ion adsorption using groundnut shell powder.

Table 4 lists the constants of the IPD kinetic model that were determined from the graphs. The regression values were high, and the model suited the adsorption process well. According to the findings, the Pseudo first and second order, Elovich and IPD kinetic models accurately describe the adsorption process and show that the adsorption mass transfer mechanism follows the rate-controlling step with external film diffusion.

3.12. Influence of temperature

The temperature of metal ions in aqueous solutions affects the effectiveness of metal ion absorption by the adsorbent. The temperature of the metal ion solution was changed from 15 to 60°C in this batch mode of investigation, and the influence of the quantity of metal ion absorption by the groundnut shell charcoal powder was investigated.

The concentration of metal ion solution was set at 25 mg L^{-1} with a 60-minute equilibrium duration. The temperature influence was discovered using 2.5 g L^{-1} of ground nut shell adsorbent. Figure 16 demonstrates that as the temperature rises from 15°C, the amount of metal ion adsorption progressively increases, and a gradual reduction is noticed at 30°C. Metal ion adsorption was reduced at 30°C due to an increased desorption rate (Aswini *et al.,* 2019). Furthermore, the exothermic nature of adsorption of adsorption IPD reduces metal ion absorption due to the small size of the adsorbent surface.
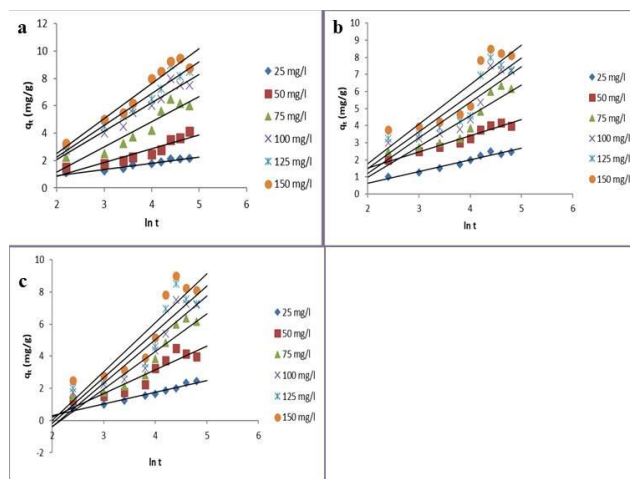

Figure 14. Elovich kinetic plots of (a) Cu, (b) Pb and (c) Hg metal ion adsorption using groundnut shell powder.
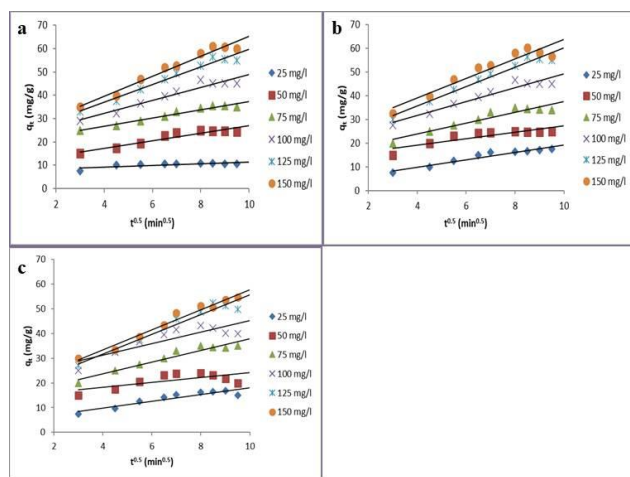

Figure 15. IPD kinetic plots of (a) Cu, (b) Pb and (c) Hg metal ion adsorption using groundnut shell powder.

Table 5. Thermodynamic constants for metal ion uptake using groundnut shell charcoal powder

Cu metal ion Concentration (Initial) in mg L^{-1}	Enthalpy (ΔH°) KJ mol^{-1}	Entropy (ΔS°) J mol^{-1}	Gibbs Energy (ΔG$_o$) kJ mol^{-1}			
			15°C	30°C	45°C	60°C
25	73.519	196.024	-13.106	-9.580	-8.362	-7.472
50	41.822	101.345	-9.856	-8.532	-7.649	-6.328
75	24.825	51.552	-7.362	-6.338	-6.037	-5.824
100	17.564	34.824	-6.125	-5.832	-5.015	-4.923
125	14.724	31.283	-5.724	-5.245	-4.992	-4.325
150	12.271	27.834	-4.762	-4.524	-4.327	-4.081
Pb metal ion Concentration (Initial) in mg L^{-1}						
25	45.434	113.234	-11.298	-9.438	-8.834	-6.683

50	31.298	75.582	-9.462	-7.736	-7.336	-6.026
75	18.362	37.725	-8.642	-6.224	-5.906	-5.124
100	15.182	31.923	-6.766	-5.835	-5.215	-4.853
125	12.837	24.846	-5.833	-5.053	-4.723	-4.257
150	10.699	19.274	-5.032	-4.636	-4.224	-4.003
Hg metal ion Concentration (Initial) in mg L^{-1}						
25	34.623	80.832	-9.102	-7.792	-7.068	-6.491
50	21.392	42.292	-8.432	-6.923	-6.226	-5.345
75	18.696	37.143	-6.692	-5.724	-5.162	-4.346
100	12.823	26.882	-6.078	-5.026	-4.622	-4.028
125	11.180	22.174	-5.121	-4.224	-4.098	-3.946
150	9.984	19.924	-4.446	-4.012	-3.925	-3.281

Table 6. Desorption of metal ions from the spent adsorbent using sulfuric acid

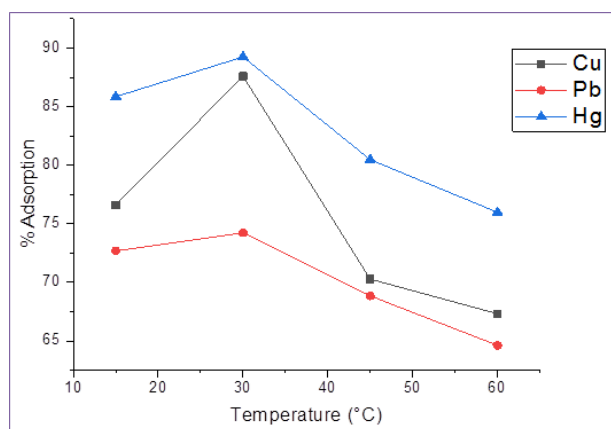| Initial concentration (25 mg L^{-1})	Recovery of metal ions (%)	Concentration of H_2SO_4			
		0.10 N	0.20 N	0.30 N	0.40 N
		% Desorption of metal ions			
Cu	98.25	89.26	93.57	93.82	91.31
Pb	87.72	80.93	83.25	83.94	81.84
Hg	81.18	71.73	74.58	75.23	73.83

Figure 16. Influence of temperature in metal ion adsorption.

3.13. Thermodynamic studies

Figure 17 depicts thermodynamic graphs using the log Kc vs 1/T relationship in different metal ion trace levels from 25 to 150 mg L^{-1}. It is essential to find the ΔH° and ΔS° values from the slope and deflection calculation. The importance of entropy and enthalpy changes were obtained from the linear plots and represented in Table 5. The Gibbs energy (ΔG°) values are negative with positive enthalpy changes (ΔH°) values, confirming that the adsorption reaction follows an endothermic response due to the impulsive nature of groundnut shell charcoal powder adsorbent (Rui *et al.*, 2020).
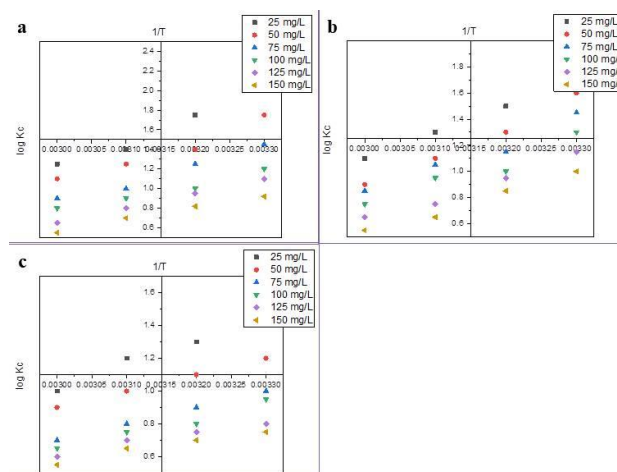

Figure 17. Thermodynamic plots of (a) Cu, (b) Pb and (c) Hg metal ion adsorption using groundnut shell powder.

3.14. Desorption studies

The spent adsorbent from batch investigations was recovered by adding concentrated sulfuric acid ranging from 0.1 N to 0.4 N. The amount of recovery of metal ions using sulfuric acid is represented in Table 6. Referring to the values obtained from the desorption studies, the maximum amount of metal ions was recovered using 0.3 N sulfuric acid. Furthermore, when the concentration of sulfuric acid has increased, the decrease in metal ion recovery has reduced. The desorption is directly proportional to the exhausted adsorbent and its capacity to release metal ions (Ye *et al.*, 2019). No metal ion recovery was obtained to increase the concentration of sulfuric acid. Hence, 0.3 N of sulfuric acid was fixed as an optimum value for recovering metal ions from the spent adsorbent.

4. Conclusions

The batch adsorption study was conducted to check groundnut shell powder's metal ion uptake behaviour as an adsorbent material. The characterization studies such as BET, SEM, EDX, FTIR & XRD confirm the availability of active sites and structure of activated groundnut shell powder. At 30°C optimum temperature, the Langmuir, Freundlich, R-P & Sips isotherms followed the adsorption process by the monolayer mechanism. The kinetic studies of Pseudo 1st and 2nd orders, Elovich, and IPD models were fitted well with the adsorption process by a heterogeneous mechanism with external film diffusion. By adding 0.3 N of concentrated sulfuric acid, the maximum number of metal ions recovered from the used adsorbent was reached. Thermodynamic studies confirm the endothermic nature of the adsorption process between adsorbent and adsorbate, and the spent metal ions have been recovered using concentrated sulfuric acid. According to the results of the preceding experiments, the groundnut shell can better absorb metal ions from aqueous solutions.

Declaration of competing interest

The authors declare that they have no known competing financial interests or personal relationships that could have appeared to influence the work reported in this paper.

References

Al-Baidhani J.H., and Al-Salihy S.T. (2016). Removal of heavy metals from aqueous solution by using low cost rice husk in batch and continious fluidized experiments. *International Journal of Chemical Engineering and Applications*, 7, 6–10.

Alghamdi A.A., Al-Odayni A-B., Saeed W.S., Al-Kahtani A., Alharthi F.A., and Aouak T. (2019). Efficient adsorption of lead (II) from aqueous phase solutions using polypyrrole – based activated carbon. *Materials*, 12, 1–16.

Al-Harby N.F., Albahly E.F., and Mohamed N.A. (2021). Kinetics, isotherm and thermodynamic studies for efficient adsorption of congo red dye from aqueous solution onto novel cyanoguanidine-modified chitosan adsorbent. *Polymers*, 13, 4446.

Ali A., Saeed K., and Mabood F. (2016). Removal of Chromium (VI) from aqueous medium using chemically modified banana peels as efficient low-cost adsorbent. *Alexandria Engineering Journal*, 55, 2933–2942.

Al-Salehin P.Z., Moeinpour F., and Mohseni-Shahri F.S. (2019). Adsorption isotherm and thermodynamic studies of As (III) removal from aqueous solutions using used cigarette filter ash. *Applied Water Science*, 9, 172.

Aswini K., and Jaishankar V. (2019). Adsorption treatment of heavy metal removal from simulated wastewater using rice husk activated carbon and its polyvinylpyrrolidoone composite as an adsorbent. *Journal of Water and Environmental Sciences*, 3, 460–470.

Cobbina S.J., Duwiejuah A.B., and Quainoo A.K. (2019). Single and simultaneous adsorption of heavy metals onto groundnut shell biochar produced under fast and slow pyrolysis. *International Journal of Environmental Science and Technology*, 16, 3081–3090.

Dulla J.B., Tamana M.R., Boddu S., Pulipati K., and Srirama K. (2020). Biosorption of copper (II) onto spent biomass of Gelidiella acerosa (brown marine algae): optimization and kinetic studies. *Applied Water Science*, 10, 56.

Edet U.A., and Ifelebuegu A.O. (2020). Kinetics, isotherms, and thermodynamic modeling of the adsorption of phosphates from model wastewater using recycled brick waste. *Processes*, 8, 665.

Feszterová M., Porubcová L., and Tirpáková A. (2021). The monitoring of selected heavy metals content and bioavailability in the soil-plant system and its impact on sustainability in agribusiness food chains. *Sustainability*, 13, 7021.

Frutos I., García-Delgado C., and Gárate A. (2016). Biosorption of heavy metals by organic carbon from spent mushroom substrates and their raw materials. *International Journal of Environmental Science and Technology*, 13, 2713–2720.

Gopal N., Asaithambi M., Sivakumar P., and Sivakumar V. (2016). Continious fixed bed adsorption studies of rhodamine – B dye using polymer bound adsorbent. *Indian Journal of Chemical Technology*, 23, 53–58.

Guo T., Bulin C., Li B., Zhao Z., Yu H., Sun H., Ge X., and Xing R. (2018). Efficient removal of aqueous Pb (II) using partially reduced graphene oxide-Fe3O4. *Adsorption Science & Technology*, 36, 1031–1048.

Idris S., Iyaka Y.A., Dauda B.E.N., Ndamisto M.M., and Umar M.T. (2012). Kinetic study of utilizing groundnut shell as an adsorbent in removing chromium and nickel from dye effluent. *American Chemical Science Journal*, 2, 12–24.

Indhumathi P., Syed Shabudeen P.S., Shoba U.S., and Saraswathy C.P. The removal of chromium from aqueous solution by using green micro algae. *Journal of Chemical and Pharmaceutical Research*, 6, 799–808.

Jan S.U., Ahmad A., Khan A.A., Melhi S., Ahmad I., Sun G., Chen C-M., and Ahmad R. Removal of azo dye from aqueous solution by a low-cost activated carbon prepared from coal: adsorption kinetics, isotherms study, and DFT simulation. *Environmental Science and Pollution Research*, 28, 10234–10247.

Jiao C., Cheng Y., Fan W., and Li J. (2012). Synthesis of agar – stabilized nanoscale zero valent iron particles and removal study of hexavalent chromium. *International Journal of Environmental Science Technology*, 12, 1603–1612.

Kalavathy M.H., Karthikeyan T., Rajgopal S., and Miranda L.R. (2014). Kinetic and isotherm studies of Cu (II) onto HPO-activated rubber wood sawdust. *Journal of Colloidal Interface Sciences*, 292, 54–362.

Kibami D. (2018)., Kinetics and adsorption studies of lead (II) onto activated carbon using low-cost adsorbents. *Global Nest Journal*, 20, 381–388.

Kim Y-S., and Kim J-H. (2019). Isotherm, kinetic and thermodynamic studies on the adsorption of paclitaxel onto Sylopute. *The Journal of Chemical Thermodynamics*, 130, 104–113.

Kromah V., and Zhang G. (2021). Aqueous adsorption of heavy metals on metal sulfide nanomaterials: synthesis and application. *Water*, 13, 1843.

Lacin D., and Aroguz A.Z. (2020). Kinetic studies on adsorption behavior of methyl orange using modified halloysite, as an eco-friendly adsorbent. *SN Applied Sciences*, 2, 2091.

Mahdavi S., Salehi Z., and Zarabi M. (2020). Isotherm and kinetic studies for adsorption of boron on nano-copper oxide (CuO) in non-competitive and competitive solutions. *Desalination and Water Treatment*, 192, 259–270.

Manjuladevi M., Anitha R., and Manonmani S. (2018). Kinetic study on adsorption of Cr (VI), Ni (II), Cd (II) and Pb (II) ions from aqueous solutions using activated carbon prepared from cucumis melo peel. *Applied Water Science*, 8.

Mehdi Niknam S., Kashaninejad M., Escudero I., Teresa Sanz M., Beltrán S. , and Benito J.M. (2021). Valorization of olive mill solid residue through ultrasound-assisted extraction and phenolics recovery by adsorption process. *Journal of Cleaner Production*, **316**, 128340.

Mwandira W., Nakashima K., Kawasaki S., Arabelo A., Banda K., Nyambe I., Chirwa M., Ito M., Sato T., Igarashi T., Nakata H., Nakayama S., and Ishizuka M. (2020). Biosorption of Pb (II) and Zn (II) from aqueous solution by Oceanobacillus profundus isolated from an abandoned mine. *Scientific Reports*, **10**, 21189.

Nathan R.J., Martin C.E., Barr D., and Rosengren R.J. (2021). Simultaneous removal of heavy metals from drinking water by banana, orange and potato peel beads: a study of biosorption kinetics. *Applied Water Science*, **11**, 116.

Ouyang D., Zhuo Y., Hu L., Zeng Q., Hu Y., and He Z. (2019). Research on the adsorption behaviour of heavy metal ions by porous material prepared with silicate tailings. *Minerals*, **9**, 291.

OuYang X-K., Yang L-P. and Wen Z-S. (2014). Adsorption of Pb (II) from solution using peanut shell as biosorbent in the presence of amino acid and sodium chloride. *BioResources*, **9**(2), 2446–2458.

Pham B.N., Kang J-K., Lee C-G., and Park S-J. (2021). Removal of heavy metals (Cd²⁺, Cu²⁺, Ni²⁺, Pb²⁺) from aqueous solution using hizikia fusiformis as an algae-based bioadsorbent. *Applied Sciences*, **11**, 8604.

Pham T.T., Hoang M.T., Nguyen M.K., Dinh T.H., Han P.H., and Bruggen B.V. (2015). Evaluation of chemical modified sugarcane bagasse for cadmium removal in aqueous environment, International proceedings of chemical. *Biological and Environmental Engineering*, **88**, 6–10.

Phuengphai P., Singjanusong T., Kheangkhun N., and Wattanakornsiri A. (2021). Removal of copper (II) from aqueous solution using chemically modified fruit peels as efficient low-cost biosorbents. *Water Science and Engineering*, **14**, 286–294.

Raghav S., and Kumar D. (2018). Adsorption equilibrium, kinetics, and thermodynamic studies of fluoride adsorbed by tetrametallic oxide adsorbent. *Journal of Chemical & Engineering Data*, **63**, 1682–1697.

Rai M.K., Shahi G., Meena V., Meena R., Chakraborty S., Singh R.S.,and Rai B.N. (2016). Removal of hexavalent chromium Cr (VI) using activated carbon prepared from mango kernel activated with H3PO4. *Resource-Efficient Technologies*, **2**, S63–S70.

Renu, M.A., Singh K., Gupta R., and Dohare R.K. (2020). Continious fixed bed adsorption of heavy metals using biodegradable adsorbent: Modelling and experimental study. *Journal of Environmental Engineering*, **146**, 04019110.

Rudi N.N., Muhamad M.S., Chuan L.T., Alipal J., Omar S., Hamidon N., Hamid N.H.A., Sunar N.M., Ali R., and Harun H. (2020). Evolution of adsorption process for manganese removal in water via agricultural waste adsorbents. *Heliyon*, **6**, e05049.

Sanchez-Machado D.I., Lopez-Cervantes J., Correa-Murrieta Ma.A., and Sanchez-Duarte R.G. (2016). Modelling of breakthrough curves for aqueous iron (III) adsorption on chitosan –sodium tripolyphosphate, *Water Science and Technology*, **74**, 2297–2304.

Senthil Kumar P, Ethiraj H., Venkat A., Deepika N., Nivedha S., Vidhyadevi T., Ravikumar L., and Sivanesan S. (2017). Adsorption, kinetic, equilibrium and thermodynamic investigations of Zn (II) and Ni (II) ions removal by poly

(azomethinethioamide) resin with pendent chlorobenzylidine ring. *Polish Journal of Chemical Technology*, **3**, 100–109.

Shahrokhi-Shahraki R., Benally C., El-Din M.G., and Park J. (2021). High efficiency removal of heavy metals using tire-derived activated carbon vs commercial activated carbon: Insights into the adsorption mechanisms. *Chemosphere*, **264**.

Shan R., Shi Y., Gu J., Wang Y., and Yuan H. (2020). Single and competitive adsorption affinity of heavy metals toward peanut shell-derived biochar and its mechanisms in aqueous systems. *Chinese Journal of Chemical Engineering*, **28**, 1375–1383.

Sivakumar D. (2015). Hexavalent chromium removal in a tannery industry wastewater using rice husk siica. *Global Journal of Environmental Science and Management*, **1**, 27–40.

Sruthi K.M., and Pavithra M.P. (2018). A Study on utilization of groundnut shell as biosorbent for heavy adsorption metals removal. *International Journal of Engineering and Techniques*, **4**, 411–415.

Venkatraman Y., and Priya A.K. (2021). Removal of heavy metal ion concentrations from the wastewater using tobacco leaves coated with iron oxide nanoparticles. *International Journal of Environmental Science and Technology*. **19**, 2721–2736.

Witek-Krowaik A., Szafran R.G., and Modelski S. (2011). Biosorption of heavy metals from aqueous solutions onto peanut shell as a low-cost biosorbent. *Desalination*, **265**, 126–134.

Yogeshwaran V., and Priya A.K. (2021). Experimental studies on the removal of heavy metal ion concentration using sugarcane bagasse in batch adsorption process. *Desalination and Water Treatment*, **224**, 256–272.

Yunnen C., Ye W., Chen L., Lin G., Jinxia N., and Rushan R. (2017). Continuous fixed-bed column study and adsorption modeling: Removal of arsenate and arsenite in aqueous solution by organic modified spent grains. *Polish Journal of Environmental Studies*, **26**, 1847–1854.